STRESS ANALYSIS OF THREE DIMENSIONAL TWISTED BLADES USING THE SLENDER BAR METHOD

Alexandre Karroum

A MAJOR TECHNICAL REPORT

in

The Department

of

Mechanical Engineering

Presented in Partial Fulfilment of the Requirements for
the Degree of Master of Engineering at
Sir George Williams University
Montreal, Canada

April, 1973

ABSTRACT

The function of blades in turbomachines is described and the need for an accurate stress analysis is emphasized. Due to the inherent complexity of the blade geometry most of the available analytical methods make many simplifying assumptions. Three of these methods, namely, the simple beam theory, the finite element techniques and the experimental stress analysis are outlined briefly in this report. A technique known as the slender bar method which provides a powerful tool for stress analysis of curved beams is described in detail with all relevant equations. The feasibility of this method is demonstrated by examples.

The blade geometry, equilibrium conditions and compatability equations are expressed using vector formulation. The procedure of applying the slender bar method to three dimensional twisted blades is explained and recommendations for analyzing the stresses in the blade in general are outlined. Curve fitting required for this method is also described.

RESUME

Le rôle joué par les ailettes de Turbines est décrit, et le besoin d'une analyse précise des contraintes est mis en lumière. A cause de la complexité de la gèométrie des ailettes, la plupart des méthodes analytiques disponibles font plusieurs suppositions pour simplifier le problème. Trois de ces méthodes, notamment, la théorie des poutres simples, la méthode des elements finis et des méthodes experimentales d'analyse des contraintes sont décrites brièvement dans ce rapport. Une technique connue sous le nom de "méthode des barres minces" pour l'analyse des contraintes dans les ailettes à trois dimensions est ici décrite et la faisabilité de cette méthode est démontrée par des exemples.

La géométrie de la blade, les conditions d'équilibre et les équations d'équilibre, sont exprimées, en notation vectorielle. La procédure pour appliquer la méthode des barres minces est expliquée, et des recommendations pour analyser les contraintes dans les ailettes sont donées. Les lissages nécessaires à la méthode, sont aussi inclus.

ACKNOWLEDGEMENT

The author wishes to express his profound gratitude to his thesis supervisors, Dr. M.O.M. Osman and Dr. T.S. Sankar for their valuable guidance and encouragement during all phases of this study.

The author also wishes to express his thanks to his employer, United Aircraft of Canada Limited, for their encouragement and financial assistance.

TABLE OF CONTENTS

PAGE

LIST OF FIGURES

NOMENCLATURE

X, Y, Z	global coordinate system
x, y, z	local coordinate system
$\underline{i}$, $\underline{j}$, $\underline{k}$	unit vectors along the local axes
$\underline{r}$	position vector with respect to the global coordinate axes
s	length, or distance between two points along the bar axis
f	parametric function, with subscript indicating the dependent variable
$\underline{\tau}$, $\underline{n}$, $\underline{b}$	unit vectors forming the principal triad. $\underline{\tau}$ is the unit tangent vector, $\underline{n}$ is the unit normal vector and $\underline{b}$ is the unit binomial vector
k	curvature of the blade axis
χ	twist of the blade axis
ϕ	angle between $\underline{n}$ the normal unit vector and the maximum principal axis of inertia of the blade cross-section
$\underline{\Omega}$	Daraboux vector, a vector which represents the rate at which the principal triad rotates as one moves along the blade axis
$\underline{\omega}$	vector representing the rate at which the principal axes of inertia of the blade cross-section rotate as one moves along the blade axis
p, q, r	components of the vector $\underline{\omega}$ along the local axes x, y, z
$\underline{D}$	displacement vector of a point on the blade axis
u, v, w	components of the displacement vector $\underline{D}$ along the local axes
$\underline{\theta}$	rotation vector of a point on the blade axis
α, β, γ	components of the rotation vector $\underline{\theta}$ along the local axes

$\underline{V}$	vector representing the stretching of the blade axis
$\underline{F}$	vector representing the applied force per unit length on an element of blade
$\underline{M}$	vector representing the applied torque per unit length on an element of blade
$\underline{R}$	the reaction force vector at a blade cross-section
$\underline{T}$	the reaction couple vector at a blade cross-section
I	moment of inertia of a blade cross-section, with subscript indicating direction
J	polar moment of inertia of a blade cross-section
E	Young's modulus of elasticity
G	Shear modulus of rigidity
ν	Poisson's ratio
σ	stress, with subscript indicating kind or direction

CHAPTER I

INTRODUCTION

CHAPTER I

INTRODUCTION

1.1 GENERAL REMARKS

Turbomachines obtain their motive power from the change of momentum of fluid flowing over a curved vane, called the blade. The fluid, while moving over the curved surface of the blade, exerts a pressure on the blade due to its centrifugal force. This centrifugal pressure acts normal to the blade surface and along the whole length of the blade. The resultant of the centrifugal pressure plus the effect of change of velocity is the motive force on the blade.

The torque or turning power applied by the blade to the driven machine, usually a generator, is governed by the rate of flow and the change in energy level of the fluid between the inlet and outlet of the blade. Thus, for the energy to be transferred efficiently, the whirl has to be reduced to a minimum, zero if possible, at the exit of the rotor. Excessive residual whirl reduces the efficiency of the exhaust system and tends to produce cavitation, as well as vibration in the draft tube. These are known to have a detrimental effect on the draft tube [2].*

---

* Numbers in square brackets refer to the list of references given at the end of the report.

To make the fluid exert equal work at all positions along the blade, and to ensure that the flow enters the draft tube (or exhaust duct) with a minimum possible whirl velocity, the guide vanes and the blades are twisted. The blades are designed to possess a stagger angle greater at the tip than at the root. Figure 1 shows schematically, a typical blade configuration for a gas turbine.

It is clear that the blade is the basic component of any turbomachine. The design of blades is based mainly on hydrodynamic considerations, with a trend towards the use of aerofoil shape. In order to meet all the design requirements, the blade has generally a very complicated shape and is often difficult to manufacture.

Improperly designed blades are susceptible to large deformations as well as fracture [3]. Increasing the blade thickness to reduce the stresses adds more weight which in turn, contributes to additional centrifugal forces. Therefore, it is vitally important that the design of a blade must be based on an accurate calculation of stresses.

A turbine blade is normally subjected to a combination of loading which could be divided into three types:

(i) centrifugal forces

(ii) bending stresses due to steady component of fluid flow, and

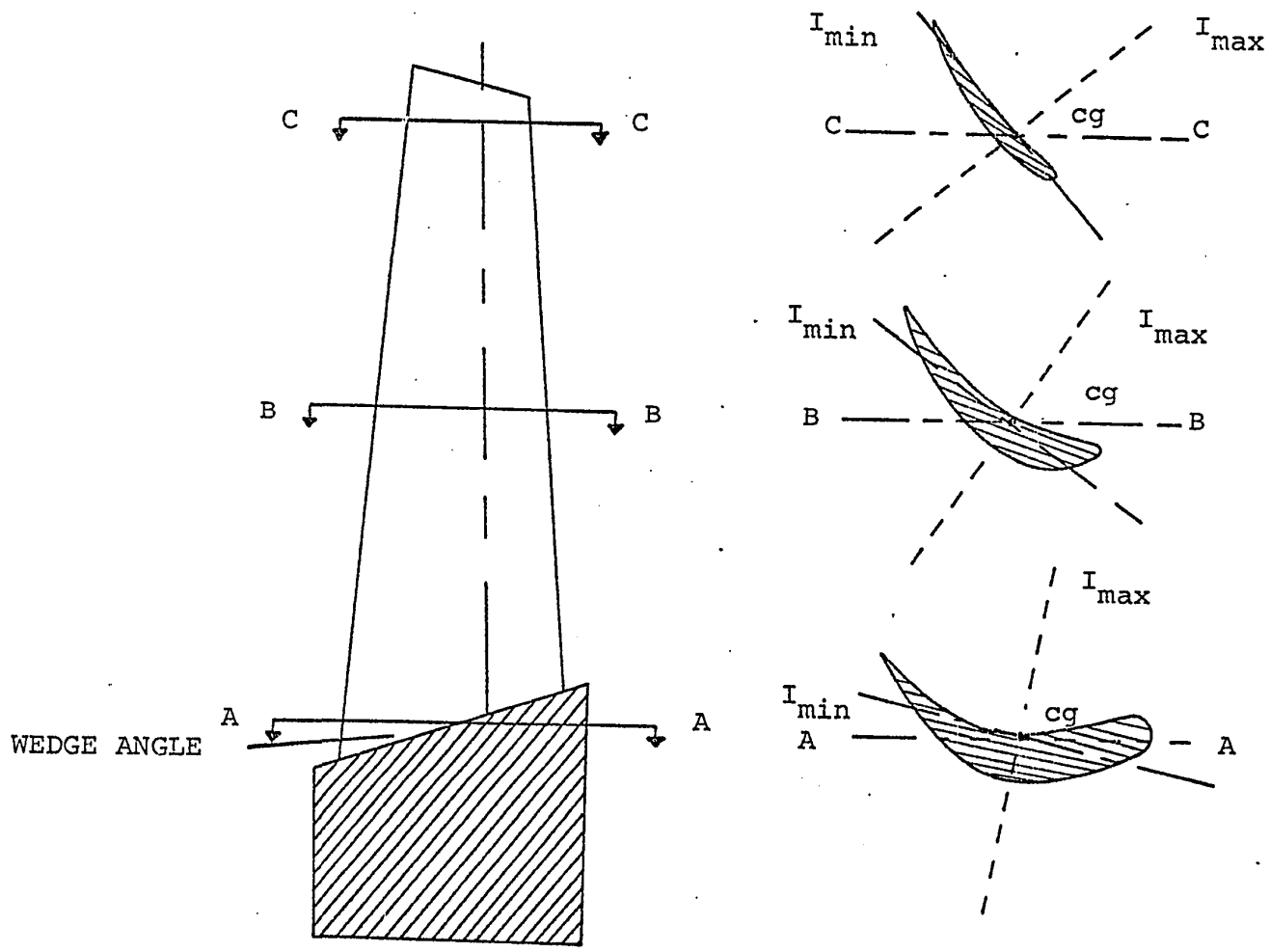

FIG. 1 A TYPICAL BLADE CONFIGURATION FOR A GAS TURBINE

(iii) vibratory bending stresses due to fluctuation in fluid pressure.

The stresses due to (iii) is generally taken as a function of the stresses due to (ii). For high output machines, external forces reach high values and induce considerable stresses in the blade. Further, the vibratory bending stresses induce high cycle fatigue, whereas, the fluctuation of the machine load or speed will cause low cycle fatigue. The importance of these vibratory stresses in the determination of fatigue strength of the blades has been demonstrated by Armstrong [4,5].

The aim of the present study is to outline the importance of blade stress analysis and to describe different techniques that are presently used. One of the techniques called the slender bar method [1,6] is emphasized and presented in detail with all relevant equations. This method essentially considers a slender bar along the blade as a finite element and provides a powerful technique for the numerical analysis of blade stresses using comparatively low computing time. The method is demonstrated using the examples of (i) a curved beam under transverse forces, (ii) a helical spring under axial load. Conclusions and recommendations are given and future work in this area is also identified.

1.2 STRESS ANALYSIS TECHNIQUES

The objective of any blade analysis is to evolve a mathematical model as close to realities as possible, that will examine the stresses at highly loaded zones, especially at the blade platform junction. Such an analysis will give basic information on deflections and fatigue life of the blades.

The identification and evaluation of the different forces exerted ,though essential for any stress analysis, is considered out of the scope of this study as this requires considerable hydrodynamic analysis.

A large number of stress analysis techniques are available at present and are used to assist in the development of the blade to meet reliability, maximum service life, and the increasing demand for more specific power. Three techniques that are commonly employed by turbine industry are described briefly here. They are:

(i) the simple beam theory
(ii) the finite element techniques
(iii) the experimental stress analysis

1.2.1 The Simple Beam Theory

In this approach, the elastic connection between two masses is approximated by a uniform beam whose elastic

properties are averages of those of the different components. The blade is assumed to remain constant in shape and the deflection of the blade is defined by infinitismal rotations and translations of the blade sections. Formulae giving beam stresses and deflections to handle different types of loading, as well as a variety of end conditions, may be found in handbooks [7,8,9] .

The stress analysis of blades using simple beam theory is based on the following assumptions:

(i) the blade is of homogeneous material

(ii) the blade is straight, or nearly so. If slightly curved, the curvature is in the plane of bending, and the radius of curvature is at least ten times the depth.

(iii) the cross-section is uniform.

(iv) all loads and reactions are along and perpendicular to the axis of the blade.

(v) the maximum stress does not exceed the proportional limit of elasticity.

(vi) the blade is long in proportion to its depth.

(vii) the blade is not disproportionately wide.

If, for any particular case, the above assumptions are violated, then the analysis will yield results which, at best, are approximate, and sometimes may be grossly in error.

For example:

(i) The derivation of the flexure formula $\sigma = \frac{Mc}{I}$, assumes that the blade is initially straight. The effect of the curvature is to increase the stress in the inside and decrease it in the outside fibers of the beam, and shift the position of the neutral axis from the centroidal axis towards the concave or the inner side.

(ii) The flexural axis is normally assumed to be the locus of the shear centres. This may not be true for a blade with considerable pre-twist.

(iii) St. Venant's torsional stiffness constant is used when the blade is under torsion. This is true only for long blades where end conditions do not have appreciable influence on torsional stresses. Otherwise, an additional constant should be used to allow for warping constraint stiffness.

For blades with a large amount of curvature, the error involved in the use of ordinary beam formulae is considerable and curved beam formulae must be used.

From the above outline of the simple beam theory, it is clear that it is intended primarily as a simple tool for preliminary design. Thus, great precision in numerical work is not justified. For most cases, slide rule calculations

giving results to three significant figures are sufficiently precise [8]. The use of the simple beam theory for preliminary blade analysis requires the engineer's judgment, and it is impossible to lay down rigid rules of procedure.

1.2.2 The Finite Element Technique

The finite element method is extensively used for the analysis of structures such as dams, buildings, aircraft and ship structures, etc... [10]. Although the method was originally developed for structural problems, it is a mathematical technique with a wide range of applications. New understanding of the concept, and the development of a wide range of finite elements make this technique a major tool for general stress and vibration problems, heat and fluid flow analysis, and recently, for problems in transients [10,11].

In a finite element analysis, the physical object, in this case the blade, is idealized into an elementary system for which a solution is available. However, the accuracy of the analysis of the idealized system in relation to the actual structure depends largely on the type of element chosen. This imposes certain constraints on the flexibility available in modeling the structure. The model will then consist of a number of elements obtained by means of fictitious cuts through the original structure. These elements are considered to be connected to each other

at the common points called nodes.

The next step of the analysis, is to compute the element stiffness matrix for each finite element. These are derived from the concept that, when the structure is deformed due to external loads, the continuity between neighbouring elements be maintained at the common nodes. Nodal point forces are expressed in terms of nodal point displacements, and the nodal point displacements are determined through the equilibrium conditions at the nodes. Using the connectivity information, the elemental stiffness matrices may be assembled into a total stiffness matrix for the object using the principle of superposition. The analysis then consists of solving a set of simultaneous equations in the form

$$[K]\{\delta\} = \{F\}$$

where $[K]$ is the total stiffness matrix, $\{\delta\}$ is the nodal displacement and $\{F\}$ is the nodal force.

Different types of elements such as triangular, rectangular, etc... have been developed to suit various types of applications. A list of these types may be found in any textbook dealing with finite elements [10,11]. The analysis also permits handling of models consisting of different types of elements. Fig. 2 shows an example of a representation of a particular tubine blade through a set of triangular finite elements. Because the turbine blades have a compli-

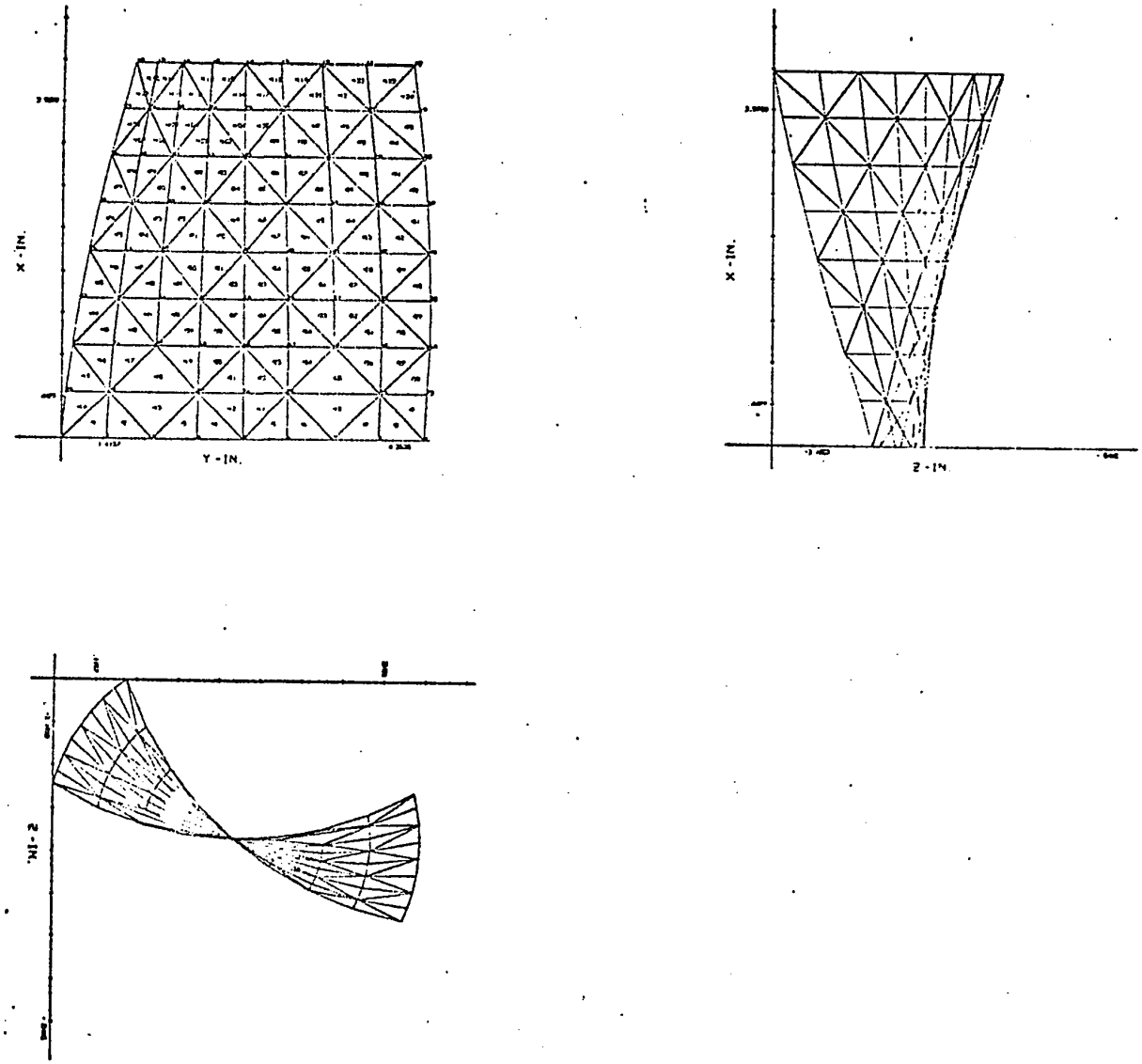

FIG. 2 REPRESENTATION OF A TURBINE BLADE THROUGH A SET OF TRIANGULAR FINITE ELEMENTS

cated shape, elements that can represent highly distorted shapes are usually required. Isoparametric elements formed by the degeneration of a three-dimensional solid have been found to give excellent solutions for twisted blades [12], since the arbitrary curved shape of the element models closely the turbine blades.

The fluid pressure, which could be considered as a distributed load, is replaced by equivalent concentrated nodal point loads. The boundary conditions are dealt with much better by the finite element technique than by any other purely analytical method.

Another attribute to this technique is that it can handle inhomogenous and anisotropic materials, by allowing each element to have its own set of specified properties. This is vital for the future application of fibrous materials in the manufacture of blades. A critical part of this method involves the solution of a large system of simultaneous linear equations. In general, the capability of such a tool is limited only by the memory capacity of the computer and the time required to complete the computational phase. Two major aspects to be considered are the accuracy of the final answers and the time and labour involved in obtaining the results [5].

1.2.3 Experimental Stress Analysis

A complete theoretical solution for the stress distribution in a blade is almost impossible. Whatever may be the method of analysis, the stress in some areas of the blade will be underestimated while at the other areas, it will be overestimated. This is mainly because of the discrepancies between the actual blade and the mathematical model. Secondly, the methods of analysis are valid only within certain limitations and are applicable only to certain types of models. To assess these theoretical methods, as well as to determine stresses at critical zones of the blades, one has to rely on experimental stress analysis. The experimental technique is also capable of detecting weaknesses, flaws unusual wear or fatigue in the blade due to defects in manufacturing.

The most direct way of determining the stress produced under a given loading is to measure the accompanying strain. Direct strain measurements are possible by mechanical and electrical pickup devices, such as extensometers, strain gauges, brittle lacquers, photogrids and cathetometers. The exact procedure and the relative merits of different experimental evaluation of stresses may be found in any standard texts [8,13] on this subject.

Under conditions of uniaxial tension or compression, it is sufficient to measure strains in one direction,

whereas, under conditions of combined stresses, it will be necessary to measure strains in more than one direction, preferably in the direction of principal stresses. In the latter cases, brittle lacquer coatings are very convenient, as they graphically present an overall strain picture, including the principal strain directions. The method consists of coating the specimen with lacquer, which becomes brittle on hardening. When the strains in the blade reach a prescribed magnitude, the surface elongation will produce cracks in the coating at a right angle to the principal tensile strain. This method gives quantitative results that are accurate to within ± 10%, and can be used to detect static and dynamic strains in tension or compression. In the case of turbine blades, stress concentration occurs around the junction between the blade and the hub. Identification of these stress concentration zones and their magnitudes are easily done through stress coating techniques. Since the stress concentrations are usually 300% greater than the overall figure,the brittle lacquer method indicates accurately the value of the stress level, as well as the direction of the principal stresses [16] .

A recent technique to be used in experimental stress analysis is holography. The successful application of the holographic non-destructive inspection is due to Leith and Upatnieks [14]. The science of holography enjoyed an active revival with the advent of the Lasar. Holographic

techniques [15] provide a method of storing three-dimensional information on a two-dimensional recording plane for subsequent viewing of the object in its original three-dimensional form. The recorded pattern called hologram bears no resemblance to the original object, but nevertheless, contains all the information about the object. The method of interferometric holography, a technique whereby minute surface deformations, in the order of microinches, induced by various stressing methods, can be detected by comparing each point on the surface with itself, before and after stressing. Interferometric holography appears to offer some promise in the detection of weaknesses, unusual wear or fatigue in turbine blades, however experimental implementation and fringe interpretation would be somewhat a time-consuming process. An experimental set-up using holographic techniques for measuring the deformation of a stressed blade is shown in Fig. 3.

In all experimental techniques described previously, the prototype is stressed and tested. There are methods such as photoelastic analysis where models are used, rather than the actual object. Information on photoelastic methods may be found in standard texts [13] on the subject.

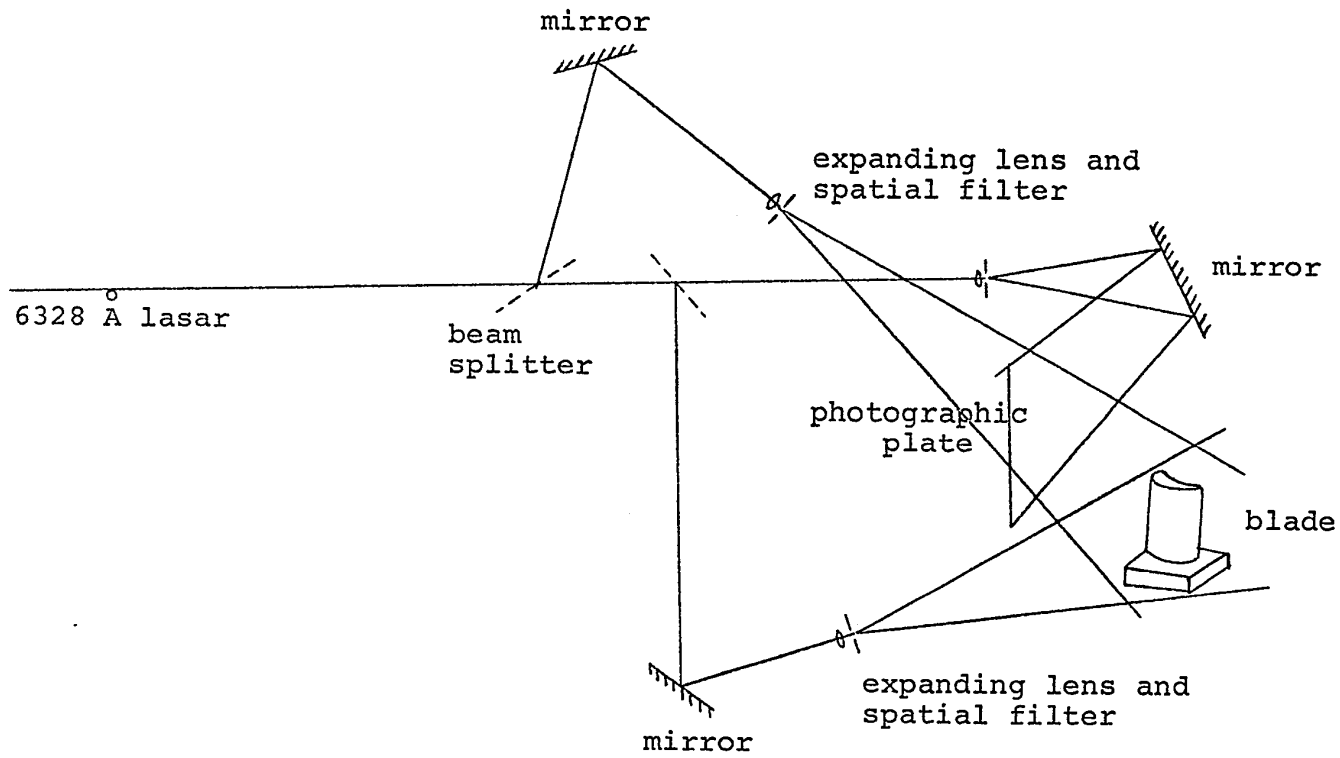

FIG. 3 SCHEMATIC REPRESENTATION OF THE HOLOGRAPHIC SET-UP USED FOR MAKING A HOLOGRAM OF A TURBINE BLADE

CHAPTER II

THE SLENDER BAR METHOD

CHAPTER II

THE SLENDER BAR METHOD

2.1 INTRODUCTION

The analysis for a twisted-curved beam involves certain added complication over that for the simple beam. When a beam is twisted and warped, the cross-sections do not remain plane. Unequal warping causes additional stresses (warping stresses) that normally occur near the fixed end. Further, the simple beam theory assumption that the flexural axis is the locus of the shear centres, is not true for pre-twisted beams. Hence, the flexural formula

$$\sigma = \frac{Mc}{I}$$

is no longer valid for curved beams.

Taking advantage of the fact that the stresses in the direction of the blade axis are much higher than the stresses in the direction perpendicular to the blade axis and employing certain approximations, the stresses in a twisted blade could be considered unidirectional. In this manner, a turbine blade could be considered as a slender tube for the purpose of stress analysis. The slender tube is then represented by a curve passing through the centroid of consecutive cross-sections. This curve will have a double curvature because of the twist in the blade and is represented through the following quantities.

(i) Curvature defined by

$$\frac{1}{\rho} = \frac{d\theta}{ds}$$

where θ is the angle to the tangent at a point on the curve and ρ is the radius of curvature.

(ii) Torsion defined by

$$\frac{1}{T} = \frac{d\eta}{ds}$$

where η is the angle between the binormals at two points separated by a distance Δs on the curve and T is known as the radius of twist of the curve.

The stress analysis technique called the slender bar method is described in detail in the following sections. This analysis is useful for calculating the stresses and deflections and also in obtaining the dynamic behaviour of the blade under centrifugal field and fluid pressure. Shroud restraint and root flexibility could also be included in this procedure.

2.2 CURVES IN SPACE

2.2.1 Definition

A space curve is a locus of points whose coordinates are functions of a single variable. Thus the coordinates

of a point P on curve C, as shown in Fig. 4, are given by a parametric equation of the type

$$\underline{r} = \underline{r}\,(s) \qquad (2.1)$$

where

$$r = r_x\underline{i} + r_y\underline{j} + r_z\underline{k}$$

$$r_x = f_x\,(s)$$

$$r_y = f_y\,(s)$$

$$r_z = f_z\,(s)$$

s is a parameter chosen to be the length measured from a reference point A on the curve.

Since

$$\lim_{\Delta s=o} \frac{|\Delta \underline{r}|}{\Delta s} = 1$$

then $\frac{d\underline{r}}{ds}$ may be defined as the unit vector along the tangent to the curve.

2.2.2 The Principal Triad

At each point on the curve, a right-handed triad may be defined, as shown in Fig. 4. The components of the triad are:

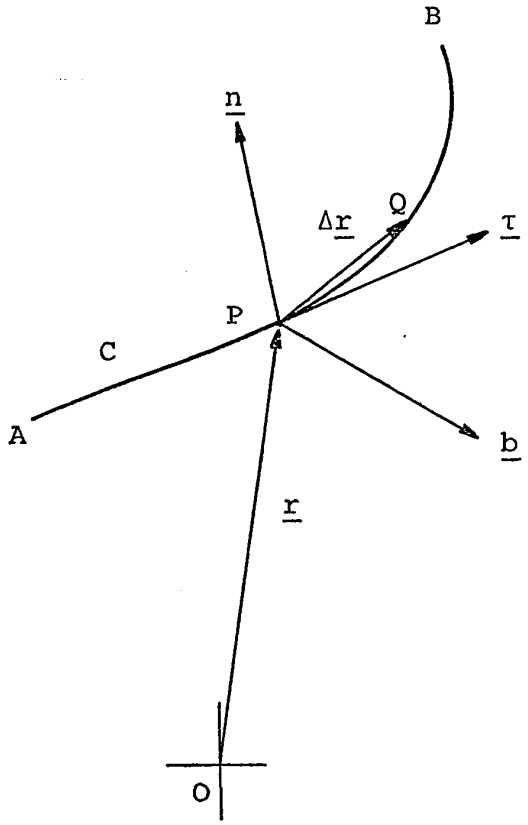

FIG. 4 ELEMENT OF A CURVE IN SPACE SHOWING THE POSITION VECTOR AND THE PRINCIPAL TRIAD

(i) $\underline{\tau}$ is a unit vector tangent to the curve at the point P under consideration and defined as positive in the direction of increasing s. This is defined as

$$\underline{\tau} = \frac{d\underline{r}}{ds} \tag{2.2}$$

$\underline{\tau}$ is called the unit tangent vector.

(ii) $\underline{n}$ is a unit vector normal to $\underline{\tau}$, and defined by

$$\frac{d\underline{\tau}}{ds} = k\underline{n} \tag{2.3}$$

$\underline{n}$ is called the unit normal vector describing the directional change in $\underline{\tau}$. k is a constant to be defined later.

(iii) $\underline{b}$ is the unit binormal vector, and forms a right-handed system with $\underline{\tau}$ and $\underline{n}$. This is defined by

$$\underline{b} = \underline{\tau} \times \underline{n} \tag{2.4}$$

The triad formed by these vectors is called the principal triad. The plane passing through P and perpendicular to $\underline{\tau}$ is called the normal plane. The plane passing through P and perpendicular to $\underline{n}$ is called the osculating plane.

For a twisted curve, the principal triad rotates about $\underline{\tau}$ as the point P moves along the curve.

2.2.3 Curvature and Twist of a Slender Bar

Eq. (2.3) defines both k and $\underline{n}$. k is the magnitude of the vector $\frac{d\underline{\tau}}{ds}$ and is called the curvature.

The binormals to a set of points on a plane curve are normal to the plane of the curve and are parallel to each other along the curve.

For a curve twisted out of its plane, the binormals will continually change directions depending on the degree of twist of the curve. The rate of change of direction of the binormals defines the curve twist and is given by the expression

$$\chi = \lim_{\Delta s=o} \frac{\eta}{\Delta s} \qquad (2.5)$$

where η is the angle between two successive binormals shown in Fig. 5, corresponding to an incremental displacement Δs on the curve.

From Fig. 5, one can see that

$$\Delta\underline{b}.\underline{n} = |\Delta\underline{b}| = -\eta \qquad (2.6)$$

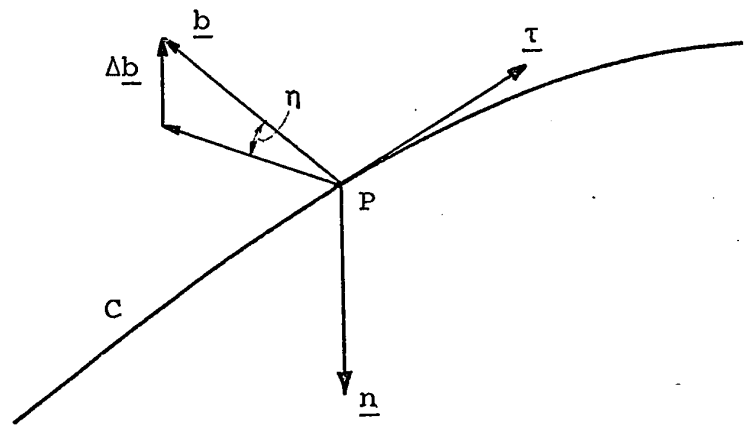

FIG. 5 DIAGRAM SHOWING THE CHANGE IN BINORMAL OF A TWISTED BLADE

Substituting this in eq. (2.5) results in

$$\chi = -\frac{d\underline{b}}{ds} \cdot \underline{n} \qquad (2.7)$$

In order to determine the curvature k and twist χ, it is necessary to express them in terms of the position vector $\underline{r}$. This is explained in the following.

From eqs.(2.2) and (2.3)

$$k = \sqrt{\frac{d^2\underline{r}}{ds^2} \cdot \frac{d^2\underline{r}}{ds^2}} \qquad (2.8)$$

Differentiating eq. (2.4)

$$\frac{d\underline{b}}{ds} = \frac{d\underline{\tau}}{ds} \times \underline{n} + \underline{\tau} \times \frac{d\underline{n}}{ds} \qquad (2.9)$$

and using in eq. (2.7), it follows

$$\chi = -\underline{n} \cdot \underline{\tau} \times \frac{d\underline{n}}{ds} \qquad (2.10)$$

Differentiating eq. (2.3)

$$\frac{d^3\underline{r}}{ds^3} = k\,\frac{d\underline{n}}{ds} \qquad (2.11)$$

The cross-product of eqs. (2.3) and (2.11) gives

$$\frac{d^2\underline{r}}{ds^2} \times \frac{d^3\underline{r}}{ds^3} = k^2\ \underline{n} \times \frac{d\underline{n}}{ds} \qquad (2.12)$$

Therefore

$$\frac{d\underline{r}}{ds} \cdot \frac{d^2\underline{r}}{ds^2} \times \frac{d^3\underline{r}}{ds^3} = -\ k^2\overline{n}\ .\ \overline{\tau} \times \frac{d\overline{n}}{ds} \qquad (2.13)$$

From eqs. (2.10) and (2.13), it may be shown that

$$\chi = \frac{1}{k^2}\left[\frac{d\underline{r}}{ds} \cdot \frac{d^2\underline{r}}{ds^2} \times \frac{d^3\underline{r}}{ds^3}\right] \qquad (2.14)$$

Eqs. (2.8) and (2.14) indicate that the curvature k and the twist χ can be determined by direct differentiation of the position vector $\underline{r}$.

2.2.4 The Seret-Frenet Formulae

The Seret-Frenet formulae are a set of equations which relate the curvature parameters k and χ with the vectors, $\underline{\tau}$, $\underline{n}$ and $\underline{b}$. The formulae are given below and can be obtained from the derivatives of the components of the principal triad.

$$\frac{d\underline{\tau}}{ds} = k\underline{n} \qquad (2.3)$$

$$\frac{d\underline{b}}{ds} = -\chi\underline{n} \qquad (2.15)$$

$$\frac{d\underline{n}}{ds} = \chi\underline{b} - k\underline{\tau} \qquad (2.16)$$

2.2.5 The Daraboux Vector

The motion of the principal triad $\underline{\tau}$, $\underline{n}$, $\underline{b}$, whose origin is a point P on a spatial curve C, consists of a translation of P along the curve and the rotation of the triad about P. The rate of rotation of the triad per unit length of the curve is characterized by the Daraboux vector $\underline{\Omega}$ and is given by

$$\underline{\Omega} = \Omega_\tau \underline{\tau} + \Omega_n \underline{n} + \Omega_b \underline{b} \qquad (2.17)$$

By definition

$$\frac{d\underline{\tau}}{ds} = \underline{\Omega} \times \underline{\tau} = - \Omega_n \underline{b} + \Omega_b \underline{n}$$

Comparing with eq. (2.3)

$$\Omega_n = 0 \qquad (2.18)$$

and

$$\Omega_b = k \qquad (2.19)$$

Similarly,

$$\frac{d\underline{n}}{ds} = \underline{\Omega} \times \underline{n} = - \Omega_b \underline{\tau} + \Omega_\tau \underline{b}$$

Comparing with eq. (2.16)

$$\Omega_\tau = \chi \qquad (2.20)$$

Now, eq. (2.17) may be written as

$$\underline{\Omega} = \chi \, \underline{\tau} + k \, \underline{n} \qquad (2.17a)$$

Consider another coordinate system x,y,z with unit vectors $\underline{i},\underline{j},\underline{k}$, respectively. Let the z-axis of the new system be along the tangent to the bar, i.e., coinciding with $\underline{\tau}$ of the principal triad. Further, let x and y axes coincide with the principal axes of inertia of the bar cross-section. Then x and y axes lie on the $\underline{n}$-$\underline{b}$ plane. The new triad $\underline{i},\underline{j},\underline{k}$ is related to the principal triad by

$$\begin{Bmatrix} \underline{i} \\ \underline{j} \\ \underline{k} \end{Bmatrix} = \begin{bmatrix} \cos\phi & \sin\phi & 0 \\ -\sin\phi & \cos\phi & 0 \\ 0 & 0 & 1 \end{bmatrix} \begin{Bmatrix} \underline{n} \\ \underline{b} \\ \underline{\tau} \end{Bmatrix} \qquad (2.21)$$

where ϕ is the angle between the unit vectors $\underline{n}$ and $\underline{i}$ of the two systems of axes.

$\underline{\omega}$, the rate of rotation per unit length of the bar, for the new triad $\underline{i},\underline{j},\underline{k}$ differs from $\underline{\Omega}$ by $\frac{d\phi}{ds}$. That is,

$$\underline{\omega} = \underline{\Omega} + \frac{d\phi}{ds} \underline{k} \qquad (2.22)$$

and

$$p = \Omega_x = k \sin\phi \qquad (2.22a)$$

$$q = \Omega_y = k \cos\phi \qquad (2.22b)$$

$$r = \Omega_z + \frac{d\phi}{ds} = \chi + \frac{d\phi}{ds} \qquad (2.22c)$$

where p,q,r are the components of $\underline{\omega}$ along the new axes x,y,z. p and q are the x and y components of the curvature and r is the twist of the bar.

2.3 SMALL DEFORMATIONS OF AN INITIALLY CURVED BAR

In order to determine the drformation of a curved bar under external loading, a system of local axes x_0,y_0,z_0, with origin at P_0, is used. This system of axes is defined in Section 2.2.5 and is illustrated in Fig. 6a. The subscript 0 denotes the unstrained state. Only small deformations are considered in this analysis.

When the rod deforms, the axes x_0,y_0,z_0 will take a new position, x,y,z shown in Fig. 6b. The z-axis is taken tangentially to the strained axis of the bar. The x_0-axis would have moved along the curve P_0P and taken the position x_0'. The x-axis is then defined to be perpendicular to the z-axis in the plane of z-x_0'. The y-axis is chosen such that it forms with x and z an orthogonal set of axes in the same sense as x_0,y_0,z_0.

As one moves along the curve the triad at P_0 rotates at a rate given by $\underline{\omega_0}$, while the triad at P rotates at a rate given by $\underline{\omega}$.

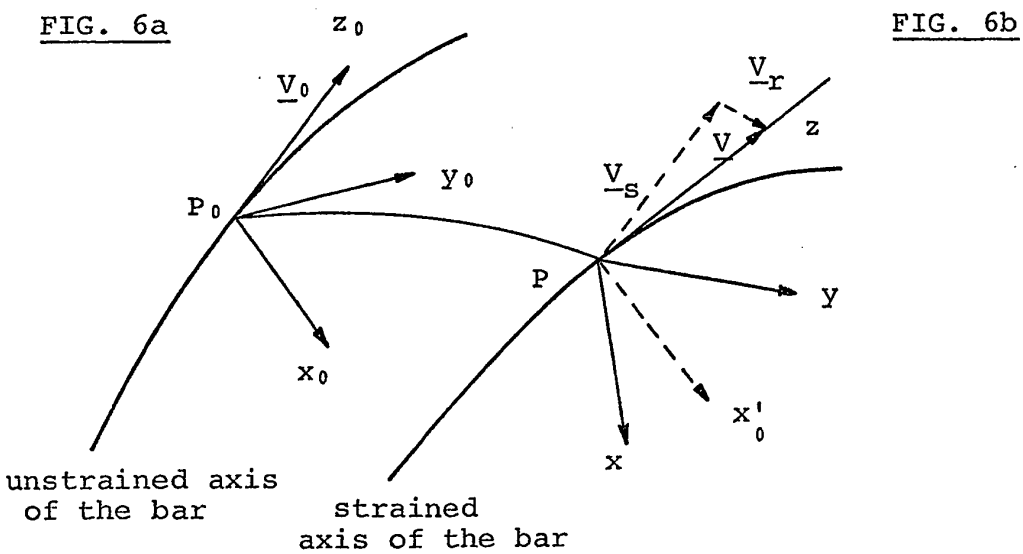

FIG. 6 DIAGRAM SHOWING THE DEFORMATION OF A BAR AXIS

Under external forces, the bar is assumed to deform slightly. Every element of the bar will undergo a small translation P_0P, given by the vector $\underline{D}$, and a small rotation given by the vector $\underline{\theta}$. The components of $\underline{D}$ in the x_0, y_0, z_0 system are defined to be u, v and w. The components of rotation $\underline{\theta}$ defined on the same reference system are α, β and γ. The triads through P_0 and P are related to each other by the rotation $\underline{\theta}$ and the relation is

$$\underline{i} = \underline{i}_0 + \underline{\theta} \times \underline{i}_0 \tag{2.23a}$$

$$\underline{j} = \underline{j}_0 + \underline{\theta} \times \underline{j}_0 \tag{2.23b}$$

$$\underline{k} = \underline{k}_0 + \underline{\theta} \times \underline{k}_0 \tag{2.23c}$$

The transformation equations expressing the relations between the two triads are then

$$\begin{Bmatrix} \underline{i} \\ \underline{j} \\ \underline{k} \end{Bmatrix} = \begin{bmatrix} 1 & \gamma & -\beta \\ \gamma & 1 & \alpha \\ \beta & -\alpha & 1 \end{bmatrix} \begin{Bmatrix} \underline{i}_0 \\ \underline{j}_0 \\ \underline{k}_0 \end{Bmatrix} \tag{2.24}$$

The stretching of the bar could be considered as if the point P is moving along the bar axis. For a unit rate of stretching $\underline{V}$, shown in Fig. 6, given by

$$\underline{V} = \underline{V}_r + \underline{V}_s \tag{2.25}$$

where $\underline{V}_r$ is the strain defined by

$$\underline{V}_r = \frac{du}{ds}\,\underline{i} + \frac{dv}{ds}\,\underline{j} + \frac{dw}{ds}\,\underline{k} \qquad (2.26)$$

and $\underline{V}_s$ is the translation of the x_0, y_0, z_0 system represented by

$$\underline{V}_s = \underline{V}_0 + \underline{\omega}_0 \times \underline{D} \qquad (2.27)$$

Referring to the system x_0, y_0, z_0, the coordinates of P are the displacements u,v,w. The direction cosines of the tangent to the bar axis at P are, from eq. (2.24), β, $-\alpha$, 1. Because $\underline{V}$ is a unit vector along the tangent, these direction cosines are also the projections of $\underline{V}$ along the x_0, y_0, z_0 axes. Therefore

$$\underline{V} = \beta\,\underline{i}_0 - \alpha\, j_0 + k_0$$

but, from eqs. (2.25), (2.26) and (2.27)

$$\begin{aligned}\underline{V} = {} & \underline{V}_0 + (q_0 w - r_0 v)\underline{i}_0 + \\ & + (r_0 u - p_0 w)\underline{j}_0 + (p_0 v - q_0 u)\underline{k}_0 + \\ & + \frac{du}{ds}\, i_0 + \frac{dv}{ds}\,\underline{j}_0 + \frac{dw}{ds}\,\underline{k}_0\end{aligned}$$

and

$$\underline{V}_0 = \underline{k}_0$$

These equations lead to a set of relations known as

the first set of Clebsch's equations and are given by

$$\beta = q_0 w - r_0 v + \frac{du}{ds} \qquad (2.28a)$$

$$-\alpha = r_0 u - p_0 w + \frac{dv}{ds} \qquad (2.28b)$$

$$0 = p_0 v - q_0 u + \frac{dw}{ds} \qquad (2.28c)$$

Following the same procedure for $\underline{\omega}$, we have

$$\underline{\omega} = \underline{\omega}_0 + \underline{\omega}_r \qquad (2.29)$$

where

$$\underline{\omega}_r = \frac{d\alpha}{ds}\,\underline{i}_0 + \frac{d\beta}{ds}\,\underline{j}_0 + \frac{d\gamma}{ds}\,\underline{k}_0$$

The projections of $\underline{\omega}_0$ and $\underline{\omega}_r$ upon the x,y,z axes may be written, using eqs. (2.24), as

$$\underline{\omega}_0 = (p_0+\gamma q_0-\beta r_0)\underline{i} + (q_0+\alpha r_0-\gamma p_0)\underline{j} +$$

$$+ (r_0+\beta p_0-\alpha q_0)\,\underline{k}$$

and

$$\underline{\omega}_r = \left(\frac{d\alpha}{ds}+\gamma\frac{d\beta}{ds}-\beta\frac{d\gamma}{ds}\right)\underline{i} + \left(\frac{d\beta}{ds}+\alpha\frac{d\gamma}{ds}-\gamma\frac{d\alpha}{ds}\right)\underline{j} +$$

$$+ \left(\frac{d\gamma}{ds}+\beta\frac{\gamma\alpha}{ds}-\alpha\frac{d\beta}{ds}\right)\underline{k}$$

Neglecting second order terms and denoting the change in curvature and twist by

$$\Delta p = p - p_0 \tag{2.30a}$$

$$\Delta q = q - q_0 \tag{2.30b}$$

$$\Delta r = r - r_0 \tag{2.30c}$$

and substituting in eq. (2.29) the values of $\underline{\omega_0}$ and $\underline{\omega}_r$ results in

$$\Delta p = \frac{d\alpha}{ds} + \gamma q_0 - \beta r_0 \tag{2.31a}$$

$$\Delta q = \frac{d\beta}{ds} + \alpha r_0 - \gamma p_0 \tag{2.31b}$$

$$\Delta r = \frac{d\gamma}{ds} + \beta p_0 - \alpha q_0 \tag{2.31c}$$

These equations determine the change in curvature and twist, and are known as the second set of Clebsch's equations. The first and second set of Clebsch's equations define completely the deformation of the bar. They are, in fact, the compatability equations.

2.4 EQUILIBRIUM OF AN ELEMENT OF THE BAR

Fig. 7 shows schematically, the free-body diagram of an element of the slender bar. The external forces applied to the element are represented by means of a force $\underline{F}$ and a couple $\underline{M}$ per unit length of the element. The components of $\underline{F}$ and $\underline{M}$ referred to the principal triad are F_x, F_y, F_z and M_x, M_y, M_z, respectively. The reactions at the ends of the element are expressed by means of a force $\underline{R}$ and a couple $\underline{T}$ acting

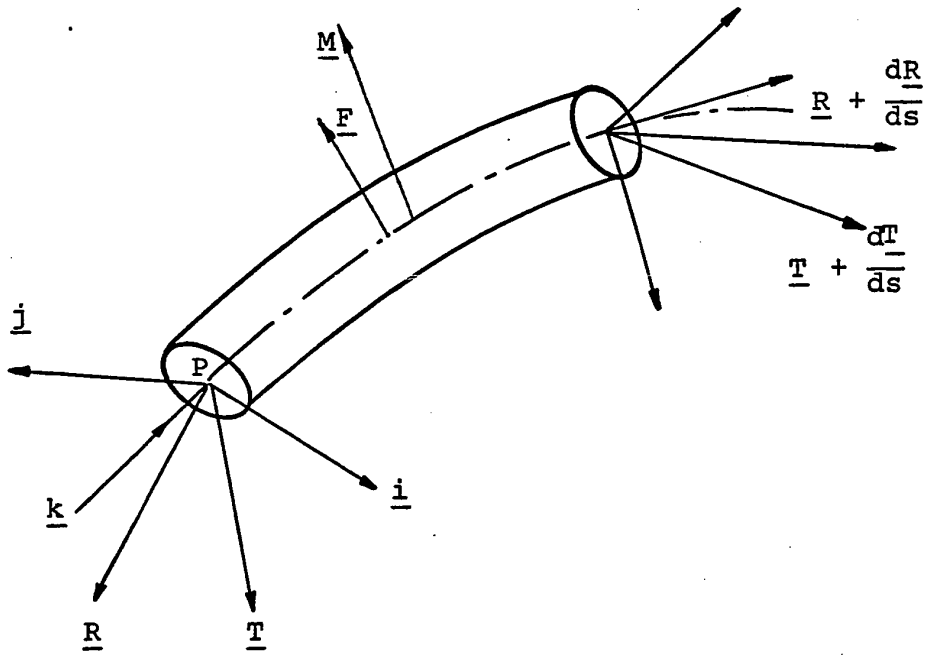

FIG. 7 FREE BODY DIAGRAM OF AN ELEMENT OF BAR

at the centroid of the section.

The element under consideration is in equilibrium if

$$\underline{F} + \frac{d\underline{R}}{ds} = 0 \tag{2.32}$$

$$\underline{M} + [\underline{\tau} \times \underline{R}] + \frac{d\underline{T}}{ds} = 0 \tag{2.33}$$

The reaction $\underline{R}$ is given by

$$\underline{R} = R_x \underline{i} + R_y \underline{j} + R_z \underline{k}$$

and its derivative is

$$\frac{d\underline{R}}{ds} = \frac{dR_x}{ds}\underline{i} + R_x \frac{d\underline{i}}{ds} + \frac{dR_y}{ds}\underline{j} + R_y \frac{d\underline{j}}{ds} + \frac{dR_z}{ds}\underline{k} + R_z \frac{d\underline{k}}{ds}$$

Since

$$\frac{d\underline{i}}{ds} = \underline{\omega} \times \underline{i} = -q\underline{k} + r\underline{j}$$

$$\frac{d\underline{j}}{ds} = \underline{\omega} \times \underline{j} = -r\underline{i} + p\underline{k}$$

$$\frac{d\underline{k}}{ds} = \underline{\omega} \times \underline{k} = -p\underline{j} + q\underline{i}$$

therefore

$$\frac{d\underline{R}}{ds} = \left(\frac{dR_x}{ds} + qR_z - rR_y\right)\underline{i} + \left(\frac{dR_j}{ds} + rR_x - pR_z\right)\underline{j} + \left(\frac{dR_z}{ds} + pR_y - qR_x\right)\underline{k} \tag{2.34}$$

Similarly one can write

$$\frac{d\underline{T}}{ds} = \left(\frac{dT_x}{ds} + qT_z - rT_y\right)\underline{i} + \left(\frac{dT_y}{ds} + rT_x - pT_y\right)\underline{j} +$$

$$+ \left(\frac{dT_z}{ds} + pT_y - qT_x\right)\underline{k} \qquad (2.35)$$

Substituting eq. (2.34) into eq. (2.32) one gets

$$\frac{dR_x}{ds} + qR_z - rR_y + F_x = 0 \qquad (2.36a)$$

$$\frac{dR_y}{ds} + rR_x - pR_z + F_y = 0 \qquad (2.36b)$$

$$\frac{dR_z}{ds} + pR_y - qR_x + F_z = 0 \qquad (2.36c)$$

Substitution of eq.(2.35)into eq.(2.33) results in

$$\frac{dT_x}{ds} + qT_z - rT_y - R_y + M_x = 0 \qquad (2.37a)$$

$$\frac{dT_y}{ds} + rT_x - pT_z - R_x + M_y = 0 \qquad (2.37b)$$

$$\frac{dT_z}{ds} + pT_y - qT_x + M_z = 0 \qquad (2.37c)$$

Eqs. (2.36) and (2.37) are known as the Kirchoff's relations which govern the equilibrium of a bar element. These six equations contain nine unknowns R_x, R_y, R_z, T_x, T_y, T_z and p,q,r.

Therefore, three additional relations between these quantities are needed. These additional equations may be obtained from the relationship between the bending moment and the curvature given by

$$T_x = EI_x \, \Delta p \tag{2.38a}$$

$$T_y = EI_y \, \Delta q \tag{2.38b}$$

$$T_z = GJ \, \Delta r \tag{2.38c}$$

Kirchoff's equilibrium eqs. (2.36) and (2.37) and Clebsch's deformation eqs. (2.28) and (2.31) provide all the information needed regarding the stress distribution and deformation of an element of slender bar under external loading.

CHAPTER III

APPLICATIONS OF THE SLENDER BAR METHOD TO THE STRESS ANALYSIS OF TWISTED BLADE

CHAPTER III

APPLICATIONS OF THE SLENDER BAR METHOD TO THE STRESS ANALYSIS OF TWISTED BLADE

3.1 GENERAL REMARKS

Stress analysis of blades may be organized into three major tasks. They are:

(i) The definition of the blade geometry.

(ii) The determination of applied hydrodynamic and centrifugal forces.

(iii) The determination of stress distribution in the blade.

The determination of hydrodynamic and centrifugal forces will be considered in this report as known quantities since they represent a certain loading condition. To define the blade geometry one needs to:

(i) Choose a suitable system of reference axes.

(ii) Divide the blade into a number of sections.

(iii) Determine the area, the centroid, the moment of inertia, as well as the principal axes for each cross-section.

(iv) Determine the radii of curvature and twist for each section.

In the following sections, the procedures for defining the blade geometry and the determination of the stress distribution in the blade are explained in detail.

3.2 DETERMINATION OF THE BLADE GEOMETRY

3.2.1 Blade Reference Axes

To relate all the different aspects of the problem, a global coordinate system is needed as reference. Any type of coordinate system could be used. In this analysis a right-handed Cartesian system of axes are chosen, such that:

(i) The Z-axis is along the axis of rotation of the blade and is considered positive in the direction of flow.

(ii) The X-axis is normal to the Z-axis and passes by the blade root.

(iii) The Y-axis is perpendicular to the plane containing X and Z axes such that the three axes form a right-handed system.

The definition of such a set of global axes is indicated schematically in Fig. 8.

3.2.2 Definition of the Blade Axis

To be able to apply the slender bar method, an analytical expression of the blade axis is required. This expression is in the form of the parametric equations

$$x = f_x(s) \tag{3.1a}$$

$$y = f_y(s) \tag{3.1b}$$

$$z = f_z(s) \tag{3.1c}$$

where s is the distance along the blade axis. Curve fitting may be used to determine the functions $f_x(s)$, $f_y(s)$, and $f_z(s)$. It is shown in the appendix that for this type of analysis Chebyshev polynomials possess the most suited form for expressing these functions. This is mainly because of the ease with which Chebyshev polynomials could be differentiated and integrated. To determine s, the distance along the blade axis, several points are selected along the blade,as shown in Fig. 8. These points should be as many as possible and preferably, though not necessarily, be equally spaced. The coordinates of these points are obtained from the design drawing of the blade. The length s at any particular point is given by

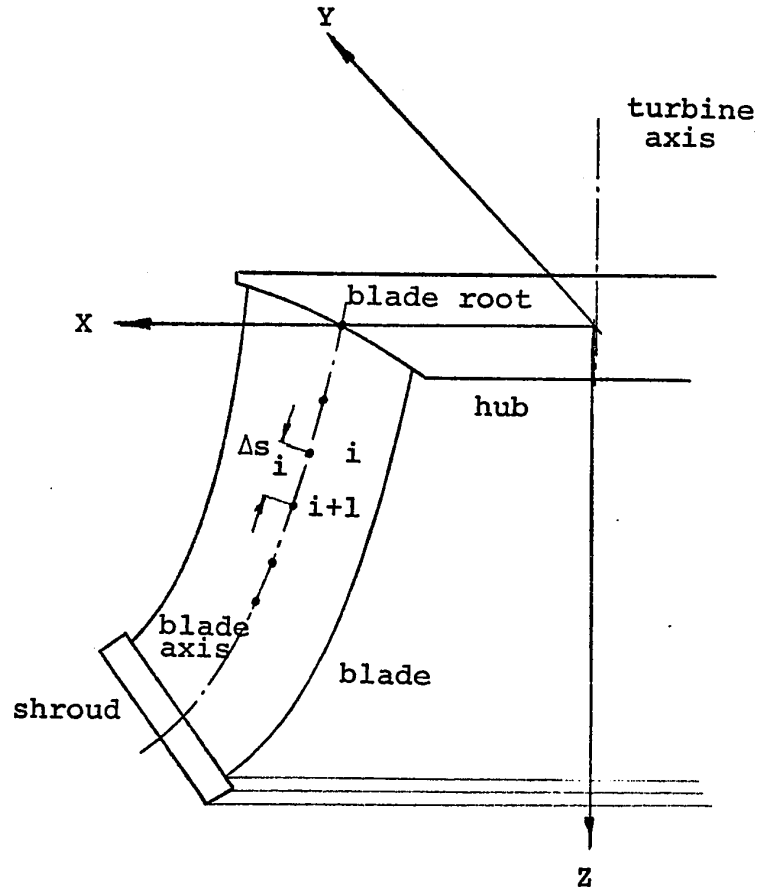

FIG. 8 FRANCIS TURBINE RUNNER SHOWING THE GLOBAL COORDINATE SYSTEM

$$s_i = \sum_{n=1}^{n=i} \Delta s_n \tag{3.2}$$

where

$$\Delta s_n = \sqrt{(x_{n+1} - x_n)^2 + (y_{n+1} - y_n)^2 + (z_{n+1} - z_n)^2}$$

3.2.3 Definition of Curvature and Twist of the Blade

At each point along the axis, the blade section properties such as area, moments of inertia, principal axes, etc.... are determined, so are the curvature k and twist χ. From eq. (2.8)

$$k = \sqrt{f''^2_x + f''^2_y + f''^2_z} \tag{3.3}$$

and from eq. (2.14)

$$\chi = \frac{1}{k^2} \begin{vmatrix} f'_x & f'_y & f'_z \\ f''_x & f''_y & f''_z \\ f'''_x & f'''_y & f'''_z \end{vmatrix} \tag{3.4}$$

The principal triad is then given from eqs. (2.2),(2.3) and (2.4) as

$$\underline{\tau} = f'_x \, \underline{i} + f'_y \, \underline{j} + f'_z \, \underline{k} \tag{3.5a}$$

$$\underline{n} = \frac{1}{k}\left(f''_x\,\underline{i} + f''_y\,\underline{j} + f''_z\,\underline{k}\right) \tag{3.5b}$$

$$\underline{b} = \frac{1}{k}\begin{vmatrix} \underline{i} & j & \underline{k} \\ f'_x & f'_y & f'_z \\ f''_x & f''_y & f''_z \end{vmatrix} \tag{3.5c}$$

Now that the principal triad and the principal axes of inertia are known at each section, the angle ϕ between the normal $\underline{n}$ and the maximum principal axis of the section can be found. The angle ϕ is then a function of s. The analytical expression for the relation between s and ϕ can be found using curve fitting.

The rate $\underline{\omega}$ with which the principal axes rotate as one moves along the blade can be found from eq. (2.22), namely

$$\underline{\omega} = p\,\underline{i} + q\,\underline{j} + r\,\underline{k} \tag{3.6}$$

where

$$p = k \sin\phi$$

$$q = k \cos\phi$$

$$r = \chi + \frac{d\phi}{ds}$$

Any change in $\underline{\omega}$ will be caused by the applied bending stresses as explained in Section (2.4).

3.3 THE EQUILIBRIUM AND COMPATABILITY EQUATIONS

Since the loading on the blade due to hydrodynamic and centrifugal forces do not produce bending, eqs. (2.32) and (2.33) become

$$\frac{d\underline{R}}{ds} = - \underline{F} \tag{3.7}$$

$$\frac{d\underline{T}}{ds} + [\underline{k} \times \underline{R}] = 0 \tag{3.8}$$

By analogy between stress and strain one can write

$$\frac{d\underline{\theta}}{ds} = \underline{\delta} \tag{3.9}$$

$$\frac{d\underline{D}}{ds} + [\underline{k} \times \underline{\theta}] = 0 \tag{3.10}$$

where $\underline{\delta}$ is the change in curvature and $\underline{D}$ is the displacement.

To be able to perform the analysis numerically, an integral form of the above four equations is more convenient than a differential form. Thus, the above equations may be written as

$$\underline{R} = \underline{R}_0 - \int_{s_0}^{s} \underline{F}\, ds \tag{3.7a}$$

$$\underline{T} = \underline{T}_0 - \int_{s_0}^{s} [\underline{k} \times (\underline{R}_0 - \int_{s_0}^{s} \underline{F}\, dt)]\, ds \tag{3.8a}$$

$$\underline{\theta} = \underline{\theta}_0 + \int_{s_0}^{s} \underline{\delta}\, ds \tag{3.9a}$$

$$\underline{D} = \underline{D}_0 + \int_{s_0}^{s} [\underline{k} \times (\underline{\theta}_0 + \int_{s_0}^{s} \underline{\delta}\, dt)]ds \tag{3.10a}$$

where $\underline{R}_0, \underline{T}_0, \underline{\theta}_0, \underline{D}_0$ are the initial values of $\underline{R}, \underline{T}, \underline{\theta}$ and $\underline{D}$ respectively. Since $\underline{k}$ is the tangent unit vector

$$\int_{s_0}^{s} \underline{k}\, ds = \underline{\ell} - \underline{\ell}_0 \tag{3.11}$$

From eq. (3.7a)

$$\int_{s_0}^{s} [\underline{k} \times \underline{R}]\, ds = \int_{s_0}^{s} [\underline{k} \times (\underline{R}_0 - \int_{s_0}^{s} \underline{F}\, dt)]\, ds \tag{3.12a}$$

Applying Dirichelet formula, eq. (3.12a) could be written as

$$\int_{s_0}^{s} [\underline{k} \times \underline{R}]\, ds = (\underline{\ell} - \underline{\ell}_0) \times \underline{R}_0 - \\ - \int_{s_0}^{s} [\underline{\ell}(s) - \underline{\ell}(t)] \times \underline{F}(t)\, dt \tag{3.12}$$

Similarly

$$\int_{s_0}^{s} [\underline{k} \times \underline{\theta}]\, ds = (\underline{\ell} - \underline{\ell}_0) \times \underline{\theta}_0 +$$

$$+ \int_{s_0}^{s} [\underline{\ell}(s) - \underline{\ell}(t)] \times \underline{\delta}(t)\, dt \qquad (3.13)$$

Substituting these values in eqs. (3.7a), (3.8a), (3.9a) and (3.10a), and resolving the vectors $\underline{R}, \underline{T}, \underline{\theta}$ and $\underline{D}$ into three components with respect to the principal axes, x, y, z, we have

$$R_x = R_{0_x} - \int_{s_0}^{s} F_x\, ds \qquad (3.14a)$$

$$R_y = R_{0_y} - \int_{s_0}^{s} F_y\, ds \qquad (3.14b)$$

$$R_z = R_{0_z} - \int_{s_0}^{s} F_z\, ds \qquad (3.14c)$$

$$T_x = T_{0_x} - (y-y_0)R_{0_z} + \int_{s_0}^{s} (y-y(t))F_z(t)\, dt \qquad (3.15a)$$

$$T_y = T_{0_y} - (x-x_0)R_{0_z} - \int_{s_0}^{s} (x-x(t))F_z(t)\, dt \qquad (3.15b)$$

$$T_z = T_{0_z} - (x-x_0)R_{0_y} + (y-y_0)R_{0_x} +$$

$$+ \int_{s_0}^{s} \{[x-x(t)]F_y(t) - [y-y(t)]F_x(t)\}dt \qquad (3.15c)$$

$$\theta_x = \theta_{0_x} + \int_{s_0}^{s} EI_x\, T_x\, ds \qquad (3.16a)$$

$$\theta_y = \theta_{0_y} + \int_{s_0}^{s} EI_y\, T_y\, ds \qquad (3.16b)$$

$$\theta_z = \theta_{0_z} + \int_{s_0}^{s} GJ\, T_z\, ds \qquad (3.16c)$$

$$D_x = D_{0_x} + (y-y_0)\theta_{0_z} - \int_{s_0}^{s} [y-y(t)]GJT_z(t)\ dt \qquad (3.17a)$$

$$D_y = D_{0_y} + (x-x_0)\theta_{0_z} + \int_{s_0}^{s} [x-x(t)]GJT_z(t)\ dt \qquad (3.17b)$$

$$D_z = D_{0_z} - (x-x_0)\theta_{0_y} + (y-y_0)\theta_{0_x} -$$

$$- \int_{s_0}^{s} \{[x-x(t)]EI_y\ T_y(t) -$$

$$- [y-y(t)]EI_x\ T_x(t)\}\ dt \qquad (3.17c)$$

In eqs. (3.15) and (3.17) t is a dummy variable, since the integrations are performed between limits. All the other variables which are not functions of t are considered as constants in these integrations.

It is recommended that numerical techniques such as Simpson's rule or Gauss-Legendre Quadrature [17,18] be used when performing the integrations. The use of computer facilities removes the tediousness of the method and allows the use of more points along the blade axis, which will then lead to accurate results.

The twelve eqs. (3.14 to (3.17) are the relations which govern the equilibrium and compatability conditions of the blade. These equations represent Clebsch's and Kirchoff's equations given by eqs. (2.28), (2.31), (2.37) and (2.38) in a different form.

The solution of these equations leads to the determination of the reactions and deflections at any section of the blade when the boundary conditions are specified. The boundary conditions required in this analysis are (i) the conditions at the blade root, and (ii) the condition at the blade tip.

CHAPTER IV

ILLUSTRATIVE EXAMPLES

CHAPTER IV

ILLUSTRATIVE EXAMPLES

To determine the feasibility and the application of the slender bar method, two examples are considered.

(i) Determination of the stress distribution in a beam initially bent in the form of a circular arc due to a load normal to the plane containing the arc.

(ii) The stress distribution in a helical spring due to a tensile axial load.

4.1 CASE STUDY 1: CURVED BEAM UNDER A TRANSVERSE FORCE

Figure 9 shows a beam AB curved in the form of a segment of a circle of radius a. The beam is of uniform circular cross-section. It is fixed at A and the other end B, where $\theta = \psi$, is free. The concentrated load W at B is normal to the plane containing the curved beam.

The position vector $\underline{r}$ of any point P_0 on the curved beam, as shown in Figure 9, is given by

$$\underline{r} = f_x \underline{i} + f_y \underline{j} + f_z \underline{k} \qquad (4.1)$$

where

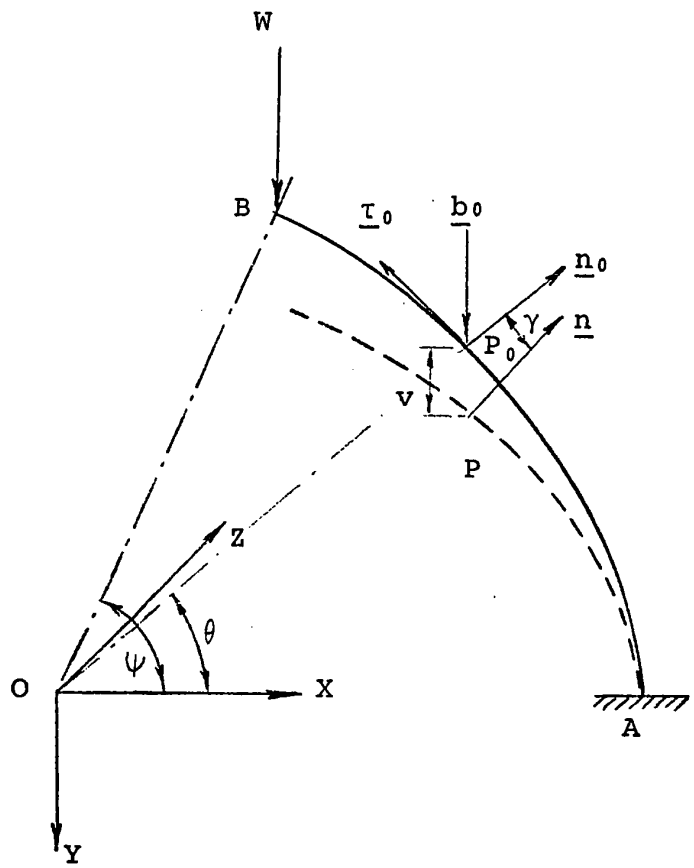

FIG. 9 DEFORMATION OF A CURVED BEAM UNDER A TRANSVERSE FORCE

$$f_x = a \cos\theta$$

$$f_y = 0$$

and

$$f_z = a \sin\theta$$

In the unstrained state, the curvature k_0 and the twist χ_0 are given by eqs. (2.8) and (2.14).

$$k_0 = \frac{1}{a} \tag{4.2a}$$

$$\chi_0 = 0 \tag{4.2b}$$

Since the beam has a uniform cross-section, the principal axes of inertia of the rod coincide with the principal triad. Therefore

$$\phi = 0 \tag{4.3}$$

In the strained state, due to deformation of the beam, the curvature and twist will change. The components of the curvature and twist along the principal axes of the deformed bar are given in terms of v the out-of-plane displacement and γ the rotation about a tangent to the beam axis. From Clebsch's eqs. (2.28) and (2.31)

$$p = \frac{\gamma}{a} - \frac{1}{a^2}\frac{d^2v}{d\theta^2} \tag{4.4a}$$

$$q = \frac{1}{a} \tag{4.4b}$$

$$r = \frac{1}{a^2}\frac{dv}{d\theta} + \frac{1}{a}\frac{d\gamma}{d\theta} \tag{4.4c}$$

Substituting the values of the curvature given by Eq. (4.4) into Kirchoff's equilibrium eqs. (2.36) and (2.37), the reactions at any section will be given, after neglecting second order terms, by

$$R_x = W\gamma \tag{4.5a}$$

$$R_y = W \tag{4.5b}$$

$$R_z = \frac{W}{a}\frac{dv}{d\theta} \tag{4.5c}$$

$$\frac{dT_x}{d\theta} + T_z - aW = 0 \tag{4.6a}$$

$$\frac{dT_y}{d\theta} - a\gamma W = 0 \tag{4.6b}$$

$$\frac{dT_z}{d\theta} - T_x = 0 \tag{4.6c}$$

The boundary conditions are such that at the free end, $\theta = \psi$

$$T_x = T_y = T_z = 0 \; . \tag{4.7a}$$

and at the fixed end $\theta = 0$

$$v = 0 \tag{4.7b}$$

$$\frac{dv}{d\theta} = 0 \tag{4.7c}$$

The simultaneous eqs. (4.6a) and (4.6b) become

$$\frac{d^2T_x}{d\theta^2} + T_x = 0$$

and

$$\frac{d^2T_z}{d\theta^2} + T_z = aW$$

The solutions to the above differential equations are

$$T_x = -aW \sin(\psi-\theta) \tag{4.8}$$

and

$$T_z = aW[1 - \cos(\psi-\theta)] \tag{4.9}$$

T_x and T_z may also be obtained from the change in curvature given by eq. (2.38)

$$T_x = EI\left(\frac{\gamma}{a} - \frac{1}{a^2}\frac{d^2v}{d\theta^2}\right) \tag{4.10}$$

$$T_z = GJ\left(\frac{1}{a^2}\frac{dv}{d\theta} + \frac{1}{a}\frac{d\gamma}{d\theta}\right) \tag{4.11}$$

From eqs. (4.9) and (4.11)

$$v + a\gamma = \frac{a^2}{GJ} \int_0^{\theta} aW\,[1 - \cos(\psi-\theta)]\,d\theta$$

$$= \frac{Wa^3}{GJ}\,[\theta + \sin(\psi-\theta) - \sin\psi] \qquad (4.12)$$

From eq. (4.8) and (4.10)

$$a\gamma = \frac{d^2v}{d\theta^2} - \frac{a^2}{EI}\,T_x$$

Substituting this in eq. (4.12), one gets

$$\frac{d^2v}{d\theta^2} + v = \frac{Wa^3}{GJ}\,[\theta + \sin(\psi-\theta) - \sin\psi] - \frac{Wa^3}{EI}\sin\,(\psi-\theta)$$

whose solution is

$$v = \frac{Wa^3}{EI}\,[\tfrac{1}{2}\theta\,\cos(\psi-\theta) - \tfrac{1}{2}\,\sin\theta\cos\psi] +$$

$$+ \frac{Wa^3}{GJ}\,[\theta - \sin\theta - \sin\psi + \sin\psi\cos\theta - \tfrac{1}{2}\sin\theta\cos\psi +$$

$$+ \tfrac{1}{2}\theta\cos(\psi-\theta)] \qquad (4.13)$$

Using this in eq. (4.12) one gets for the angular displacement γ

$$\gamma = \frac{Wa^2}{EI}\,[\tfrac{1}{2}\sin\theta\cos\psi - \tfrac{1}{2}\theta\cos(\psi-\theta) +$$

$$+ \frac{Wa^2}{GJ}\,[\sin\theta - \tfrac{1}{2}\sin\theta\cos\psi - \tfrac{1}{2}\theta\cos(\psi-\theta)] \qquad (4.14)$$

The variation of the displacements v and γ with θ are shown in Figure 10 for a curved beam having $\psi = \frac{\pi}{2}$ and $G = \frac{E}{2(1+\nu)}$.

Once the displacements are known, the reaction forces and couples can be determined at any section along the rod.

$$\left.\begin{aligned} R_x &= R_z = T_y = 0 \\ R_y &= W \\ T_x &= -\,a\,W\cos\theta \\ T_z &= a\,W\,\{1 - \cos\theta\} \end{aligned}\right\} \qquad (4.15)$$

The maximum stresses occur at the fixed end, $\theta = 0$, and they are directly computed from the reactions as follows.

$$\left.\begin{aligned} \sigma_{shear,\,max} &= \frac{16Wa}{\pi d^3} \\ \sigma_{bending,max} &= \frac{32Wa}{\pi d^3} \end{aligned}\right\} \qquad (4.16)$$

The maximum principal stress is

$$\sigma_{max} = \frac{16\sqrt{5}\,Wa}{\pi d^3}$$

where d is the diameter of the beam.

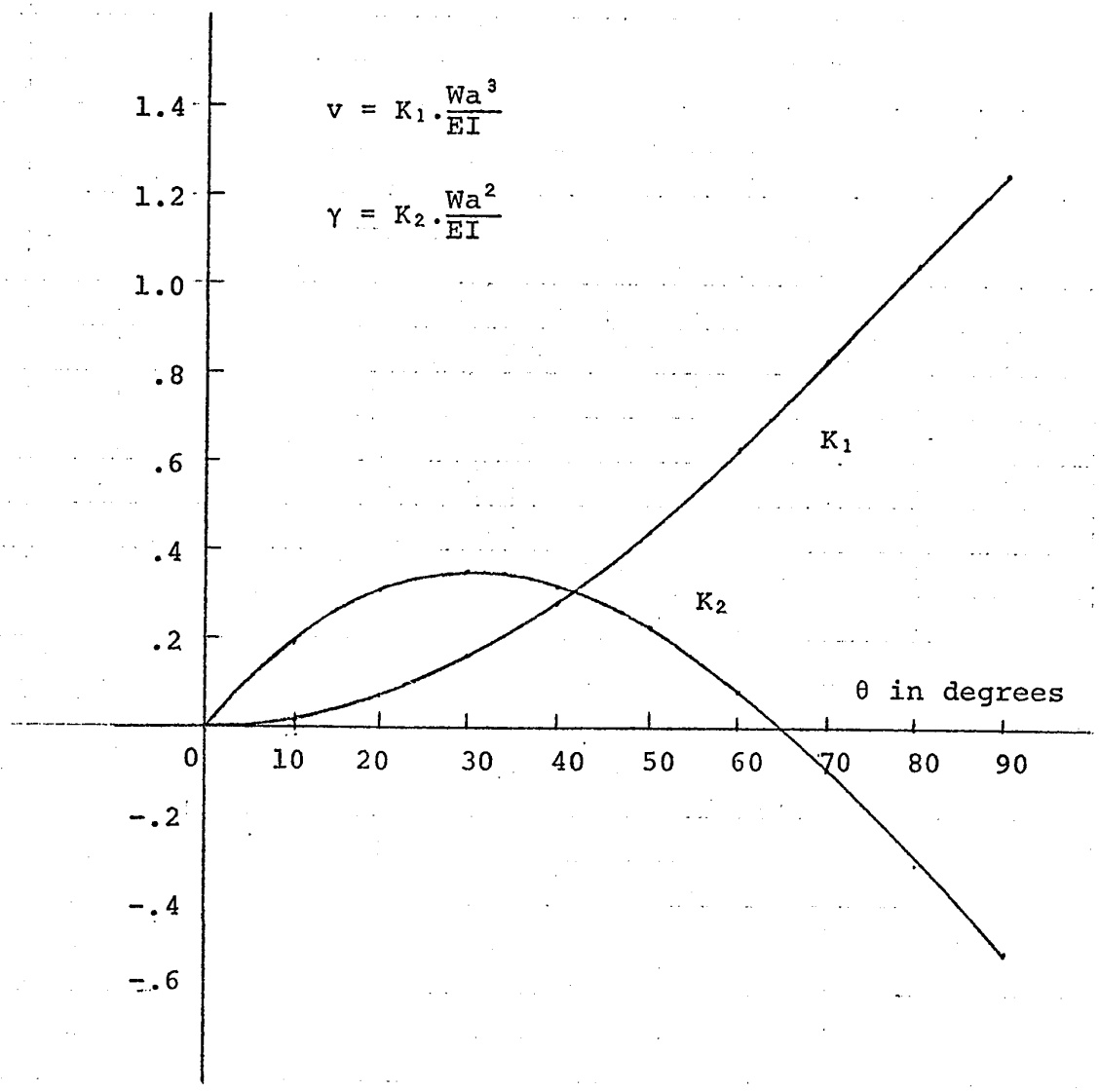

FIG. 10 VARIATION OF v AND γ WITH RESPECT TO θ FOR A CURVED BEAM

4.2 CASE STUDY 2: HELICAL SPRING UNDER TENSILE AXIAL LOAD

Figure 11 shows schematically a helical spring under an axial load W. The spring is made of a wire having a uniform circular cross-section. The axis of the wire describes a helix defined by the quantities a_0 and α_0, where a_0 is the radius of the cylinder on which the helix lies and α_0 is the angle between the tangent to the coil and a plane perpendicular to the axis of the helix.

The position vector $\underline{r}$ of any point P_0 on the spring, as shown in Figure 11, is given by

$$\underline{r} = f_x \underline{i} + f_y \underline{j} + f_z \underline{k} \tag{4.17}$$

where

$$f_x = a_0 \cos\theta$$

$$f_y = a_0 \sin\theta$$

$$f_z = a_0 \theta \sin\alpha_0$$

In the unstrained state, the curvature k_0 and the twist χ_0 are defined by the quantities

$$k_0 = \cos^2 \alpha_0 / a_0 \tag{4.18a}$$

$$\chi_0 = \sin\alpha_0 \cos\alpha_0 / a_0 \tag{4.18b}$$

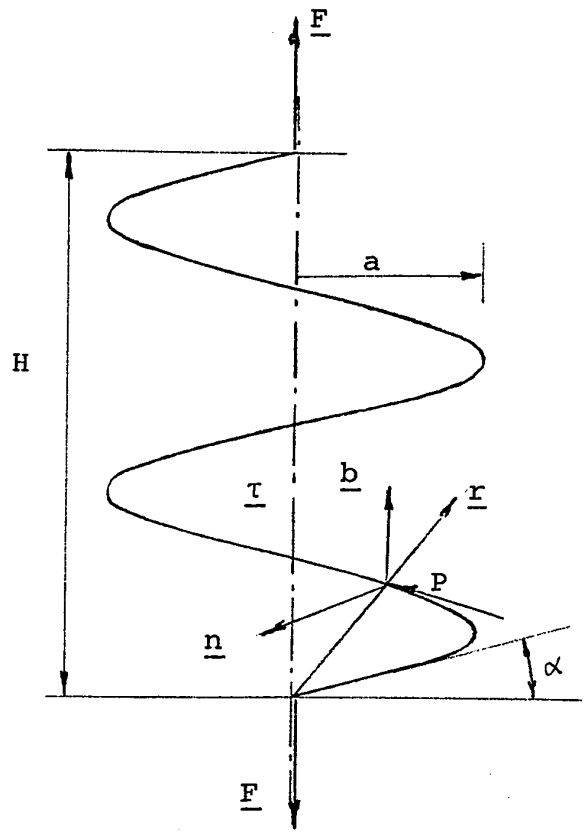

FIG. 11 HELICAL SPRING UNDER AXIAL LOAD

Since the spring wire is of uniform circular cross-section, the principal axes of inertia of the wire and the principal triad will always coincide. Hence, ϕ, the angle between the principal axis of inertia and $\underline{n}$ of the principal triad, is equal to zero.

From eqs. (2.22), the components of $\underline{\omega}_0$ are given by

$$p_0 = 0 \tag{4.19a}$$

$$q_0 = \cos^2\alpha_0/a_0 \tag{4.19b}$$

$$r_0 = \sin\alpha_0\cos\alpha_0/a_0 \tag{4.19c}$$

In the strained state,both the spring parameters a and α will change. The incremental change in curvature and twist will therefore be given by

$$\delta p = 0 \tag{4.20a}$$

$$\delta q = \delta\left(\frac{\cos^2\alpha}{a}\right) \tag{4.20b}$$

$$\delta r = \delta\left(\frac{\sin\alpha\cos\alpha}{a}\right) \tag{4.20c}$$

From eqs. (2.37), the reaction couples are

$$T_x = 0 \tag{4.21a}$$

$$T_y = EI\delta\left(\frac{\cos^2\alpha}{a}\right) \tag{4.21b}$$

$$T_z = GJ\delta\left(\frac{\sin\alpha\cos\alpha}{a}\right) \tag{4.21c}$$

From eqs. (2.36), the reaction forces are

$$R_x = 0 \tag{4.22a}$$

$$R_y = GJ\frac{\cos^2\alpha}{a}\,\delta\left(\frac{\sin\alpha\cos\alpha}{a}\right) - $$

$$- EI\,\sin\alpha\cos\alpha\,\delta\left(\frac{\cos^2\alpha}{a}\right) \tag{4.22b}$$

$$R_z = R_y\,\tan\alpha \tag{4.22c}$$

From boundary conditions, the spring reactions at the end A are given by

$$R_y = W\cos\alpha \tag{4.23}$$

$$T_z\,\sin\alpha + T_y\,\cos\alpha = 0 \tag{4.24}$$

Expressing the height H of the spring and ψ, the total angle of the coil, in terms of α, the helix angle, and ℓ, the length of the wire, we have

$$H = \ell\,\sin\alpha \tag{4.25}$$

$$\psi = \frac{\ell}{a}\cos\alpha \tag{4.26}$$

For small deformations, the change in H and ψ are expressed as

$$\delta H = \ell\,\cos\alpha\,\delta\alpha \tag{4.27}$$

$$\delta\psi = -\frac{\ell}{a}\sin\alpha\ \delta\alpha -$$

$$-\frac{\ell}{a^2}\cos\alpha\ \delta\alpha \tag{4.28}$$

Therefore,

$$\delta\alpha = \delta H/\ell\ \cos\alpha \tag{4.29}$$

$$\frac{\delta a}{a^2} = -\ (\sin\alpha\ \delta H + a\ \cos\alpha\ \delta\psi)/\ell a\ \cos^2\alpha \tag{4.30}$$

$$\delta\left(\frac{\sin\alpha\cos\alpha}{a}\right) = \cos\alpha\ \frac{\delta H}{\ell a} + \sin\alpha\ \frac{\delta\psi}{\ell} \tag{4.31}$$

$$\delta\left(\frac{\cos^2\alpha}{a}\right) = \cos\alpha\ \frac{\delta\psi}{\ell} - \sin\alpha\ \frac{\delta H}{\ell a} \tag{4.32}$$

Substituting these values in eqs. (4.22), (4.23) and (4.24)

$$W = \frac{1}{\ell a}\left[(GJ\ \cos^2\alpha + EI\ \sin^2\alpha)\,\delta H + (GJ-EI)\sin\alpha\ \cos\alpha\ a\ \delta\psi\right] \tag{4.33}$$

$$\frac{1}{\ell a}\left[(GJ-EI)\sin\alpha\ \cos\alpha\ \delta H + (GJ\ \sin^2\alpha + EI\ \cos^2\alpha)\,a\ \delta\psi\right] = 0 \tag{4.34}$$

The solution of these simultaneous equations may be written in the form

$$\delta H = W\ell\ a^2\left(\frac{\sin^2\alpha}{EI} + \frac{\cos^2\alpha}{GJ}\right) \tag{4.35}$$

and

$$\delta\psi = W\ell\ a\left(\frac{1}{GJ} - \frac{1}{EI}\right)\sin\alpha\ \cos\alpha \tag{4.36}$$

The quantity $\ell a^2\left(\frac{\sin^2\alpha}{EI} + \frac{\cos^2\alpha}{GJ}\right)$ in eq. (4.35) is the inverse of the stiffness of the spring.

Substituting the values of δH and $\delta\psi$ from eqs. (4.35) and (4.36) into eqs. (4.30) to (4.32) and then back into eqs. (4.21) and (4.22), one gets

$$T_x = 0 \tag{4.37a}$$

$$T_y = Wa \sin\alpha \tag{4.37b}$$

$$T_z = Wa \cos\alpha \tag{4.37c}$$

$$R_x = 0 \tag{4.38a}$$

$$R_y = W \cos\alpha \tag{4.38b}$$

$$R_z = W \sin\alpha \tag{4.38c}$$

The sets of eqs. (4.37) and (4.38) give the reaction forces and couples at any section of the spring. From these forces and couples, the stresses may be determined as follows, using elasticity formulae.

$$\sigma_{direct} = \frac{32W \sin\alpha}{\pi d^3} (8d + a)$$

$$\sigma_{shear} = \frac{16W}{\pi d^3} (\frac{d}{3} + a \cos\alpha)$$

and the maximum principal stress may be given by

$$\sigma_{max} = \frac{16Wa}{\pi d^3} (1 + \sin\alpha)$$

and the maximum shearing stress

$$\tau_{max} = \frac{16Wa}{\pi d^3}$$

CHAPTER V

CONCLUDING REMARKS

CHAPTER V

CONCLUDING REMARKS

In this thesis, various techniques for determining stresses in a three-dimensional curved blade are briefly explained. Out of these, the slender bar method is shown to be a powerful tool for stress analysis of curved shapes such as blades, springs, curved beams, etc. Although this method is not as accurate as the finite element method, it renders results which are sufficient for general design purposes. Also, the slender bar method yields the most accurate closed form solutions for the determination of stress distribution in twisted bodies.

The basic assumptions of the slender bar method are:

(i) The stresses in the direction of the blade axis are much higher than the stresses in the perpendicular direction. Thus, under this approximation, the stresses in a twisted blade can be considered as unidirectional.

(ii) The blade is long enough so that the end conditions do not drastically affect the stress distributions.

The procedure of stress analysis using the slender bar method consists basically of the following steps:

(i) The blade is divided into several sections. The geometric properties such as area, centroid, moment of inertia and principal axes, are determined for each section.

(ii) The section centroids are joined by a smooth curve, called the blade axis. Curve fitting is used to provide an analytical expression for the blade axis.

(iii) The blade geometry, as outlined in Chapter III, are defined.

(iv) The blade loading condition is determined from hydrodynamic consideration of the problem.

(v) Kirchoff's eqs. (2.36) and (2.37) and Clebsch's eqs. (2.28) and (2.31) are solved for the reactions and deflections at each section of the blade.

(vi) The stresses at each section of the blade are then calculated from the numerical values obtained in (v).

Two applications are given in Chapter IV of this thesis, mainly to illustrate the procedure and to demonstrate the feasibility of the method.

The shortcoming of the method lies mainly in the fact that the blade is treated as a slender rod neglecting

the effect of increase of flexural rigidity due to Poisson's effect. This beam type analysis, although good for long blades, cannot be expected to give accurate results for low aspect ratio blades. Such blades ought to be treated as a pretwisted plate, rather than as a pretwisted beam.

The slender bar method has also the potential of being used as a finite element within the body under consideration. This might provide a powerful technique for the numerical analysis of blade stresses using comparatively low computing time. However, this is subject to future investigation and justification.

APPENDIX

CURVE FITTING

APPENDIX

CURVE FITTING

The data will generally be in the form of discrete points (x_i, y_i); $i = 1,2, \ldots , n$. Usually, these points are scattered, and they may or may not be equally spaced. However, they may show a definite trend, i.e., the data might belong to a function $f(x)$ which one seeks to know. The difference r_i between the calculated value $y(x_i)$ and the given data y_i is a measure of the accuracy of the fit and is called the deviation

$$r_i = y(x_i) - y_i \qquad \text{(A.1)}$$

The topic of curve fitting deals mainly with finding a simple model $y(x)$ in the form of a series

$$y(x) = \sum_{i=o}^{i=m} a_i F_i(x) \qquad \text{(A.2)}$$

which is as close as possible to the unknown function $f(x)$. Two basic criteria are available to minimize the error.

(i) <u>The Least Square Approximation</u>

In this case, one sums all the squares of the deviation r_i at all data points. This sum is then minimized with respect to the unknown parameters a_i. This results in a set of equations called the "normal equations" which

are solved for the parameters a_i.

(ii) The Minimax Approximation

In this case, one chooses, among the class of polynomials of degree m, the one which has the least E, where E is given by

$$E = \max |r_i| \qquad (A.3)$$

Any textbook dealing with numerical analysis [17,18,19] will contain information on numerical approximation of functions. The purpose of this appendix is to brief the reader with the topic of curve fitting and to select among the different models available the one which is more suitable for representing the blade axis. Several mathematical models are used to perform the fitting; however, the best suited model for a particular problem is determined by experience. In the present case of blade axis curve fitting, Chebyshev polynomials are recommended.

In the slender bar method, a highly desired feature, is the ability to differentiate and integrate the fitted function eqs. (3.3),(3.4), etc. This could easily be achieved when Chebyshev polynomials are used. This model has other advantages, such as:

(i) The Chebyshev series has an evenly distributed error in the range of interest because of its "equal ripple property".

(ii) The Chebyshev series converges very rapidly, thus a fewer number of terms are needed to guarantee a given degree of accuracy.

(iii) When solving for the unknown coefficient a_i in eq. (A.2) it yields a well conditioned matrix.

Another point of consideration is the degree of fit. Given a number of data points (x_i, y_i); $i = 1,2,\ldots,n$, different orders of m for the approximating polynomial will yield different values of the error r_i. Evidently, as m increases, the error will decrease. However, the error will be zero, when $m = n-1$. In such a case, the fitted curve will be forced to pass through all the data points. This is highly undesirable, since all the smoothing properties of the least square approach will be lost, and the fit for the intermediate points will be inaccurate. Therefore, it is recommended to try several values of m as the order of fit, and the maximum error in each case is plotted against the value of m. The smallest value of the order m that gives an acceptable level for the error is then chosen as the best fit.

REFERENCES

REFERENCES

[1] Kovalev, N.N.,"Hydroturbines Design and Construction", translated from Russian and edited by Israel Program for Scientific Translation, Jerusalem, 1965.

[2] "The Jet Engine", Edited by Rolls-Royce, Publication Ref. T.S.D. 1302, second edition.

[3] Massoud, M.P.,"Vectorial Derivation of the Equations for Small Vibrations of Twisted Curved Beams", Trans. ASME, Journal of Applied Mechanics, June, 1965.

[4] Armstrong, E.K., and Stevenson, R.C., "Some Practical Aspect of Compressor Blade Vibration", J. Royal Aeronautical Soc., 1960.

[5] DiPrima, R.C., and Handelman, G.H., "Vibration of Twisted Beams", Quarterly of Applied Mathematics, Vol. 12, No. 3, October, 1954.

[6] Prager, W., "Theory of Structures", Brown University, mimeographed note , 1944.

[7] Eshback, W., "Handbook of Engineering Funamentals", Wiley Engineering Handbook Series, (Chapter 5).

[8] Roark, Raymond J., "Formulas for Stress and Strain", McGraw-Hill Book Co., New York.

[9] Fluge, W., "Handbook of Engineering Mechanics", McGraw-Hill Book Co., New York, 1962, (Chapter 35).

[10] Holand, Ivan and Bell, Koblein, "Finite Element Methods in Stress Analysis".

[11] Zienkiewicz, O.C., and Y.K. Chung, "The Finite Element Method in Structural and Continuum Mechanics", McGraw-Hill Book Co., New York, 1967.

[12] Ahmad, S., Anderson, R.G., and Zienkiewicz,O.C., "Vibration of Thick Curved Shells, With Particular Reference to Turbine Blades", Journal of Strain Analysis, Vol. 5, No. 3, 1970.

[13] Dally, James W., and Riley, William F., "Experimental Stress Analysis", McGraw-Hill Book Co., New York.

[14] Leith, E., and Upatnieks, J., "Wavefront Reconstruction With Diffused Illumination and Three-Dimensional

Optics", J. Opt. Soc. Am., Vol. 54, 1964, p.1295.

[15] Investivation of Applying Interferometric Holography to Turbine Blade Stress Analysis, United Aircraft Research Laboratories, Report J990798-13, February, 1970.

[16] Drew, D.A., "Developments in Methods of Measuring Stresses in Compressor and Turbine Blades on Test Bed and in Flight", Published by the Inst. Mech. Engrs.

[17] Mansour, W.M., "Introduction to Numerical Approximation of Functions", Series of Lectures given at Sir George Williams University.

[18] Mansour, W.M., "Introduction to Finite Differences, Interpolation, Differentiation and Integration", Series of Lectures given at Sir George Williams University.

[19] Scheid, F., "Numerical Analysis", Schaum's Outline Series, 1968.

[20] Timoshenko, S., and Goodier, J.N., "Theory of Elasticity", McGraw-Hill Co., New York.

[21] Timoshenko, S., "Strength of Materials", Part I, D. Van Nostrand, Inc., New York, 1940.

[22] McConnell, A.J., "Application of Tensor Analysis.

[23] Green and Zerna, "Theoretical Elasticity".

[24] Love, A.E.H., "A Treatise on the Mathematical Theory of Elasticity", Dover Publications, New York, 1944.

[25] Eisenhart, Luther Pfahler, "An Introduction to Differential Geometry".

[26] Streeter, Victor L., "Handbook of Fluid Dynamics", 1961, McGraw-Hill Co., New York.

[27] Streeter, Victor L., "Fluid Mechanics", 5th Edition, McGraw-Hill Co., New York.

[28] Buider, R.C., "Fluid Mechanics", Prentice-Hall, Inc., Chapt. 17, 4th Edition, New York, 1950.

[29] Hoer, Kenneth L., "Writing Technical Report That Communicate", A.S.E. Report No. 680195.

[30] Gupta, J.P., "Experiment or Theory - Which Comes First", E.I.C. Journal, June, 1972.

[31] Armstrong, E.K., Crowcroft, R.S., and Hunt, T.M., "Fatigue Life of Compressor Blading", Proc. Inst. Mech. Engrs. 1965-1966, Vol. 180, pt. 31.

[32] Petricone, Ralph Donald, "Vibration Characteristics and Deformation Due to Centrifugal Loading of Low Aspect Ratio Compressor Blades", Stevens Institute of Technology, Ph.D., 1970, Engineering, Aeronautical.

[33] Tyrer, Ray, "Ceramic Coatings Measure the Complex Stresses in Gas-Turbine Blades", SESA, Experimental Mechanics, August, 1972.